

# Testing the event-chain algorithm in asymptotically free models

Martin Hasenbusch

*Institut für Physik, Humboldt-Universität zu Berlin,  
Newtonstr. 15, D-12489 Berlin, Germany*

Stefan Schaefer

*John von Neumann Institute for Computing (NIC), DESY  
Platanenallee 6, D-15738 Zeuthen, Germany*

## Abstract

We apply the event-chain algorithm proposed by Bernard, Krauth and Wilson in 2009 to toy models of lattice QCD. We give a formal prove of stability of the algorithm. We study its performance at the example of the massive Gaussian model on the square and the simple cubic lattice, the  $O(3)$ -invariant non-linear  $\sigma$ -model and the  $SU(3) \times SU(3)$  principle chiral model on the square lattice. In all these cases we find that critical slowing down is essentially eliminated.

PACS numbers: 05.50.+q, 05.10.Ln, 11.15.Ha

## I. INTRODUCTION

Monte Carlo simulation of statistical field theory systems is a standard tool in their study. While the development of algorithms has a long tradition, it is still an active field and source of substantial progress. Here we test a new class of recently proposed algorithms, the so-called event-chain Monte Carlo [1–4], in systems with asymptotic freedom. In particular, we study the two-dimensional  $O(N)$  model and the chiral  $SU(N) \times SU(N)$  principal chiral model for  $N = 3$ . As a preliminary step, we simulate free field theory.

The cost of a simulation is determined essentially by two factors: the numerical cost of a single update step and the autocorrelation times  $\tau_A$  of the observables  $A$  of interest in units of these steps. The latter typically scale with a power of the correlation length  $\xi$ :

$$\tau_A \propto \xi^z. \tag{1}$$

The dynamical critical exponent  $z$  therefore characterizes the algorithm's performance close to criticality. Algorithms, such as the local Metropolis algorithm, which essentially perform a random walk in configuration space have  $z \approx 2$ , whereas for some models also update strategies whose autocorrelation times increase much slower with the correlation length have been devised. Examples are the cluster [5, 6] and multigrid [7] algorithms. They are characterized by a coherent update of a large fraction of the field variables in one step. Such advanced algorithms, however, rely on special features of the theory to be simulated and are difficult to generalize: Algorithm performance depends strongly on the model under investigation. For a new proposal, it is therefore pivotal to test it in many cases to understand better its dynamics.

An interesting new entry in the toolbox is the so-called event-chain algorithm pioneered in Ref. [1–3]. It is basically a walker on the lattice which updates the local field variable in Monte Carlo time until a so-called event occurs, with probabilities given by the theory. Then it moves to the neighboring site, which is determined by the event. The details are given below. It is remarkable that for some theories this leads to a small value of  $z$  and not to the random walk one might naively expect.

## II. EVENT DRIVEN ALGORITHM

In this section, the algorithm is discussed for a model with a single real variable at each site of the lattice. In order to apply the algorithm to more complicated models, the simple model is embedded, as we explain below. Note that the idea of embedding is also used in the case of cluster [6, 8] and multigrid [9] algorithms. To define the algorithm, one first discusses infinitesimal updates with a step size  $\epsilon > 0$ . These updates are integrated analytically, leading to the version of the algorithm that is implemented at the end.

We consider a general scalar field theory with the action

$$S([\phi]) = \sum_{x \in \Lambda} s_x(\phi_x) + \sum_{\langle x, y \rangle} s_{\langle x, y \rangle}(\phi_x, \phi_y), \quad (2)$$

where  $s_x(\phi_x)$  and  $s_{\langle x, y \rangle}(\phi_x, \phi_y)$  are functions of the real variables  $\phi_x$ . Here we consider analytic functions. However the example of hard-spheres considered in ref. [1] shows that this requirement can be relaxed. The collection of all sites of the lattice is denoted by  $\Lambda$  and  $\langle x, y \rangle$  is a pair of interacting sites. In our numerical study, we consider nearest neighbor interactions only. We require that

$$\frac{\partial s_{\langle x, y \rangle}(\phi_x, \phi_y)}{\partial \phi_x} = - \frac{\partial s_{\langle x, y \rangle}(\phi_x, \phi_y)}{\partial \phi_y} \quad (3)$$

holds for the interaction terms.

The configuration space  $\phi$  is now extended by two “lifting” variables: the position of the walker  $\tilde{x} \in \Lambda$  at which field updates are performed and the direction  $\sigma \in \{-1, 1\}$  of these changes. Both are drawn from a uniform distribution, in particular uncorrelated to the fields  $\phi$ . Let us denote an enlarged configuration by

$$X = (\phi, \sigma, \tilde{x}). \quad (4)$$

The action pertaining to a single site, keeping the fields at all other sites fixed, can be written as

$$S_x(\phi_x) = s_x(\phi_x) + \sum_y s_{\langle x, y \rangle}(\phi_x, \phi_y) \equiv \sum_{i=0}^n s_{i,x}(\phi_x), \quad (5)$$

where  $i = 0$  indicates the single site term and  $i = 1, 2, \dots, n$  labels the interaction partners  $y$  of  $\tilde{x}$ .

The enlarged configuration  $X$  is always changed. Either  $\phi_{\tilde{x}}$  is replaced by  $\phi_{\tilde{x}} + \sigma\epsilon$  or  $\sigma$  is replaced by  $-\sigma$  or  $\tilde{x}$  is replaced by one of its interacting partners  $y_i$ . The decisions are

taken for each term of the single site action (5) separately. With the standard Metropolis probability, applied to  $s_{i,\bar{x}}$

$$p_i = \min [1, \exp[-s_{i,\bar{x}}(\phi_{\bar{x}} + \sigma\epsilon) + s_{i,\bar{x}}(\phi_{\bar{x}})]] \quad (6)$$

the proposal  $\phi_{\bar{x}} + \sigma\epsilon$  is accepted. Expanding in  $\epsilon$  we get

$$p_i = \begin{cases} 1 - \sigma \frac{\partial s_{i,\bar{x}}(\phi_{\bar{x}})}{\partial \phi_{\bar{x}}} \epsilon + O(\epsilon^2) & \text{for } \sigma \frac{\partial s_{i,\bar{x}}(\phi_{\bar{x}})}{\partial \phi_{\bar{x}}} > 0 \\ 1 + O(\epsilon^2) & \text{for } \sigma \frac{\partial s_{i,\bar{x}}(\phi_{\bar{x}})}{\partial \phi_{\bar{x}}} \leq 0 . \end{cases} \quad (7)$$

The update  $\phi_{\bar{x}} + \sigma\epsilon$  is rejected, if it is rejected by at least one  $s_{i,\bar{x}}$ . If the proposal is not accepted the following is done: In the case of  $i = 0$ ,  $\sigma$  is replaced by  $-\sigma$ , while for  $i > 0$  the walker is set to the site  $y_i$ . At finite  $\epsilon$  there is a probability  $O(\epsilon^2)$  that the proposal is rejected by more than one  $s_{i,\bar{x}}$ . Hence for a sequence of  $n$  updates with  $t = n\epsilon$  finite, the probability for conflicting decisions is  $O(\epsilon)$  and hence the algorithm becomes well defined in the limit  $\epsilon \rightarrow 0$ . A proof of the correctness of the algorithm is given in the Appendix.

The algorithm that is implemented in the program is obtained by integrating infinitesimal steps over a finite fictitious time  $t$ . The probability that there is no rejection by  $s_{i,\bar{x}}$  in  $n = t/\epsilon$  subsequent steps is

$$P_i(\phi_{\bar{x}} + \sigma t \leftarrow \phi_{\bar{x}}) = \prod_{m=1}^n p_i(\phi_{\bar{x}} + m\sigma\epsilon \leftarrow \phi_{\bar{x}} + (m-1)\sigma\epsilon) . \quad (8)$$

Taking the logarithm and the limit  $\epsilon \rightarrow 0$  one arrives at

$$\ln P_i(t) = \int_0^t d\psi \min[0, -\sigma s'_{i,\bar{x}}(\phi_{\bar{x}} + \sigma\psi)] =: -\Delta E_i(t) . \quad (9)$$

Performing the integral we get

$$\Delta E_i(t) = \sigma \sum_k [s_{i,\bar{x}}(\phi_{1,k}) - s_{i,\bar{x}}(\phi_{0,k})] , \quad (10)$$

where  $k$  labels the intervals with  $\sigma s'_{i,\bar{x}}$  positive throughout within  $[\min[\phi_{\bar{x}}, \phi_{\bar{x}} + \sigma t], \max[\phi_{\bar{x}}, \phi_{\bar{x}} + \sigma t]]$ .  $\phi_{0,k}$  and  $\phi_{1,k}$  are the lower/upper and upper/lower bounds of these intervals, depending on the value of  $\sigma$ . The field  $\phi_{\bar{x}}$  is updated until the update is rejected by one of the  $s_{i,\bar{x}}$ . The times  $t_i^{(\text{event})}$  when these events occur are determined in the following way: One draws a uniform random number  $r_i \in (0, 1]$  for each  $i$  to fix  $P_i(t)$ . We arrive at Eq. (11) of [2]:

$$\Delta E_i(t_i^{(\text{event})}) = -\ln r_i , \quad (11)$$

which has to be solved for  $t_i^{(\text{event})}$ . The  $i = i_{\min}$  with the smallest  $t_i^{(\text{event})}$  makes the race:  $t^{(\text{event})} = \min_i [t_i^{(\text{event})}]$ . The field is updated  $\phi_{\tilde{x}} \rightarrow \phi_{\tilde{x}} + \sigma t^{(\text{event})}$ . For  $i_{\min} = 0$  we replace  $\sigma$  by  $-\sigma$  and  $\tilde{x}$  remains unchanged. Else, for  $i_{\min} > 0$  the walker assumes the new position  $y_{i_{\min}}$  and  $\sigma$  keeps its sign.

The algorithm evolves in a fictitious time  $t_{MC}$ . For each event the fictitious time increases as  $t_{MC} \rightarrow t_{MC} + t^{(\text{event})}$ . A sequences of updates is started at  $t_{MC} = 0$  by drawing  $\tilde{x}$  and  $\sigma$  from a uniform distribution. The sequence of updates is stopped at some fixed  $t_f$ . To this end, events are generated until  $t_{MC}$  would overshoot  $t_f$  for the first time. This last event is not taken into account in the update of the field and  $t_{MC}$  is not increased by this last  $t^{(\text{event})}$ . Instead  $\phi_{\tilde{x}} \rightarrow \phi_{\tilde{x}} + \sigma(t_f - t_{MC})$  is performed. Furthermore, measurements should be performed in equal intervals of the fictitious time. Mostly, we performed a measurement after a complete update sequences of the length  $t_{MC}$  or after a fixed number of these sequences. Note that measuring at events leads to a bias that, at least for small system sizes, can be easily seen in the averages of estimators.

In order to arrive at a formal proof of ergodicity one has to introduce some randomness in the evolution time  $t_f$ . An alternative would be to add Metropolis updates that ensure ergodicity. In our explorative study here, similar to refs. [1–3], we simply ignore this question.

### III. THE MODELS

We consider square or simple cubic lattices. The sites of the lattice are denoted by  $x = (x_0, x_1, \dots, x_{d-1})$  with  $x_i \in \{0, 1, 2, \dots, L_i - 1\}$ , where  $d$  is the dimension of the system, setting the lattice spacing to unity,  $a = 1$ . The directions of the lattice are denoted by  $\mu \in \{0, 1, \dots, d - 1\}$ . There are  $2d$  nearest neighbors  $y_i = x \pm \hat{\mu}$ , where  $\hat{\mu}$  is a unit vector in  $\mu$ -direction. In our simulations we take  $L_0 = L_1 = \dots = L_{d-1} = L$  throughout.

#### A. Free field theory

First we study the two and three-dimensional scalar field theory. It is defined by the action

$$S = \frac{1}{2} \sum_{x,\mu} (\phi_x - \phi_{x+\hat{\mu}})^2 + \frac{m^2}{2} \sum_x \phi_x^2 + \frac{\lambda}{4!} \sum_x \phi_x^4 \quad (12)$$

In the following we will only discuss the free case  $\lambda = 0$ .

Here the functions (9) are easy to evaluate. For the single site term of the action we get

$$\Delta E_0(t) = \frac{1}{2}m^2 \begin{cases} 0 & \text{for } \sigma\phi_{\tilde{x}} < 0, t < -\sigma\phi_{\tilde{x}} \\ (\phi_{\tilde{x}} + \sigma t)^2 & \text{for } \sigma\phi_{\tilde{x}} < 0, t \geq -\sigma\phi_{\tilde{x}} \\ (\phi_{\tilde{x}} + \sigma t)^2 - \phi_{\tilde{x}}^2 & \text{for } \sigma\phi_{\tilde{x}} \geq 0. \end{cases} \quad (13)$$

For  $i > 0$  we get

$$\Delta E_i(t) = \frac{1}{2} \begin{cases} 0 & \text{for } \sigma\Delta\phi_{\tilde{x},i} < 0, t < -\sigma\Delta\phi_{\tilde{x},i} \\ (\Delta\phi_{\tilde{x},i} + \sigma t)^2 & \text{for } \sigma\Delta\phi_{\tilde{x},i} < 0, t \geq -\sigma\Delta\phi_{\tilde{x},i} \\ (\Delta\phi_{\tilde{x},i} + \sigma t)^2 - \Delta\phi_{\tilde{x},i}^2 & \text{for } \sigma\Delta\phi_{\tilde{x},i} \geq 0, \end{cases} \quad (14)$$

where  $\Delta\phi_{\tilde{x},i} = \phi_{\tilde{x}} - \phi_{\tilde{x}+\hat{\mu}} = \phi_{\tilde{x}} - \phi_{y_i}$ . There is always a solution for a positive  $t$ .

## B. Non-linear $\sigma$ -model

The action of the non-linear  $O(N)$ -invariant  $\sigma$ -model is

$$S = -\beta \sum_{x,\mu} \vec{s}_x \cdot \vec{s}_{x+\hat{\mu}}, \quad (15)$$

where  $\vec{s}_x$  is a unit vector with  $N$  real components. We shall study the model for  $N = 2$  and 3. For  $N = 2$  we get the so called XY-model. It undergoes a Kosterlitz-Thouless phase transition at  $\beta_{KT} = 1.1199(1)$  [10]. For temperatures above the transition, there is a finite correlation length. At lower temperatures there is no ordering and the two-point correlation function is decaying with a power law. For references see for example [11]. For the event-chain algorithm it is useful to write the XY-model in terms of angles  $\alpha_x$ :

$$S = -\beta \sum_{x,\mu} \cos(\alpha_x - \alpha_{x+\hat{\mu}}). \quad (16)$$

The pair terms of the action are

$$s_{i,\tilde{x}} = -\beta \cos(\alpha_{\tilde{x}} - \alpha_{y_i}). \quad (17)$$

In the update,  $\alpha_{\tilde{x}}$  is incremented. The functions (9) are given in ref. [2]. To simplify the notation, let us assume  $\sigma = 1$  in the following. Let us define

$$\delta_i = \alpha_{\tilde{x}} - \alpha_{y_i} - 2m\pi, \quad (18)$$

where the integer  $m$  is chosen such that  $-\pi < \delta_i \leq \pi$ .

$$\Delta E_i(t) = \beta \begin{cases} 2n & \text{for } \delta_i < 0, \delta_i + t - 2n\pi < 0, \\ 2n + 1 - \cos(\delta_i + t) & \text{for } \delta_i < 0, \delta_i + t - 2n\pi \geq 0, \\ 2(n - 1) + \cos(\delta_i) - 1 & \text{for } \delta_i \geq 0, \delta_i + t - 2n\pi < 0, \\ 2n + \cos(\delta_i) - \cos(\delta_i + t) & \text{for } \delta_i \geq 0, \delta_i + t - 2n\pi \geq 0, \end{cases} \quad (19)$$

where the integer  $n \geq 0$  is chosen such that  $-\pi < \delta_i + t - 2n\pi \leq \pi$ . Note that  $2n$  is the contribution from  $n$  complete cycles, where  $\cos(0) - \cos(\pi) = 2$ . For an illustration see Fig. 4 of ref. [2].

For  $N = 3$  the model has a finite correlation length at any finite value of  $\beta$ . The model is asymptotically free. The divergence of the correlation length as  $\beta \rightarrow \infty$  is governed by the so called  $\beta$ -function. For a discussion of the physics of this model see for example [12].

In the literature there are a number of Monte Carlo studies of this lattice model. It can be efficiently simulated by using the cluster algorithm [13] and the multigrid algorithm [9]. Also the micro-canonical overrelaxation algorithm [14] had been applied successfully. For simulations with the worm algorithm see ref. [15]. The simulation for  $N > 2$  with the event-chain Monte Carlo algorithm is performed, by an embedding of a generalized XY model. To this end, for one sequence of updates, one picks out a pair  $(l, k)$  of components from the  $N$  components of the field. In the update, only rotations in this plane are performed. The algorithm is run as for the XY model, with the exception that in eq. (19) the prefactor  $\beta$  is replaced by  $\sqrt{s_{l,\tilde{x}}^2 s_{k,\tilde{x}}^2} \sqrt{s_{l,y_i}^2 s_{k,y_i}^2} \beta$ .

### C. $SU(N) \times SU(N)$ principal chiral model

The principal chiral model on the square lattice is defined by the action

$$S = -\beta \sum_{x,\mu} \text{Re tr } U_x U_{x+\hat{\mu}} \quad (20)$$

where  $U_x \in \text{SU}(N)$ . The action restricted to a single site is

$$S_x = -\beta \sum_{\pm\hat{\mu}} \text{Re tr } U_x U_{x+\hat{\mu}}^\dagger \equiv \sum_{i=1}^{2d} s_{x,i}. \quad (21)$$

The model is asymptotically free. For a discussion of the physics of this model see for example [16]. No efficient implementation of the cluster algorithm has been devised for this

model so far. However the multigrid algorithm has been implemented successfully [16]. To this end, for one sequence of updates a one-parameter subgroup is considered. Here we apply the same idea. Following [16], a general one parameter update can be composed of a random  $SU(N)$  rotation and a rotation by a variable angle along one, fixed element  $\lambda$  of the algebra. With

$$\lambda = \begin{pmatrix} i & 0 & \dots & \\ 0 & -i & 0 & \dots \\ 0 & \dots & & \end{pmatrix}$$

the updates read

$$U \rightarrow e^{tR\lambda R^\dagger} U = R e^{t\lambda} R^\dagger U,$$

leading to an embedded action for site  $x$  and component  $i$

$$s_{i,x}(t) = -\beta[a \cos t + b \sin t] = -\beta c \cos(t - t_0)$$

with

$$a = \text{Re}([W_i]_{11} + [W_i]_{22}) \quad \text{and} \quad b = \text{Im}([W_i]_{11} - [W_i]_{22}), \quad (22)$$

where  $W_i = R^\dagger U_x U_{y_i}^\dagger R$ . Furthermore  $c = \sqrt{a^2 + b^2}$  and  $t_0 = \arctan(b/a)$ .

#### IV. NUMERICAL RESULTS

Below we discuss our numerical results for the scalar free field theory, the  $O(3)$ -invariant nonlinear  $\sigma$ -model and the  $SU(3) \times SU(3)$ -invariant principal chiral model. We abstain from a discussion of our simulations of the two-dimensional XY-model, since our results are fully consistent with those of ref. [17].

##### A. Scalar free field theory

We simulated the Gaussian model on the square and simple cubic lattice. In our simulations, we have taken  $L \propto m^{-1}$ , evolving the fictitious Monte Carlo time for the period  $t_f$  using the event-chain algorithm. Once this is reached, a new site  $\tilde{x}$  and direction  $\sigma$  are selected. Note that  $t_f$  is the only free parameter of the algorithm.

Let us define the quantities that we measured in our simulations. The first two quantities are related to the terms in the action:

$$O_1 = \frac{1}{2dL^d} \sum_{\langle xy \rangle} (\phi_x - \phi_y)^2, \quad O_2 = \frac{1}{2L^d} \phi_x^2. \quad (23)$$

Then we determined magnetization and a proxy of the correlation length

$$O_3 = \frac{1}{2} \left( \sum_x \phi_x \right)^2, \quad O_4 = \sum_{i=0}^{d-1} \tilde{\phi}_i \tilde{\phi}_i^* \quad (24)$$

with the Fourier transform  $\tilde{\phi}_i = \sum_x \exp(-i2\pi x_i/L) \phi_x$ .

In the Gaussian model, all these quantities can be easily computed exactly by Fourier transformation. We compared the outcome of our simulations with these exact results. The largest deviation had been 3.4 standard deviations for a single observable.

We performed a measurement after  $n_m$  sequences of the length  $t_f$ . For a given  $L$  we kept  $t_{\text{meas}} = n_m t_f$  constant. It is chosen such that the integrated autocorrelation times in units of  $t_{\text{meas}}$  are of  $O(10)$ .

### 1. Two dimensions

In the two-dimensional case we simulated the linear lattice sizes  $L = 32, 64, 128,$  and  $256$ . Correspondingly the masses are taken as  $m = 0.3, 0.15, 0.075,$  and  $0.0375$ , respectively. Each series of simulations consists of  $10^6$  measurements, separated by  $t_{\text{meas}} = 100, 400, 2000$  and  $8000$  for  $L = 32, 64, 128,$  and  $256$ , respectively. We focus on the dependence of the autocorrelations on the length  $t_f$  of the update sequence.

In Fig. 1 we give the integrated autocorrelation time of  $O_3$ , while for the other observables the results are listed in table I. Since the cost of the simulation scales with  $L^2$  at least, the autocorrelation times are given in units of  $L^2$ . This means that the autocorrelation times in units of measurements are divided by  $32^2/100, 64^2/400, 128^2/2000, 256^2/8000$ , respectively. Plotting the autocorrelation time as a function of  $t_f/L^2$ , we see a reasonable collapse of the data for the four different lattice sizes. We conclude that  $t_f$  should be chosen such that  $t_f \propto m^{-2} \propto L^2$ . The integrated autocorrelation time of  $O_3$  decreases with increasing  $t_f$  and seems to approach a plateau value for large  $t_f$ . We can not exclude that  $\tau$  increases for very large  $t_f$  again, we will see an example below in the principle chiral model. Here we will not examine  $t_f > L^2$ .

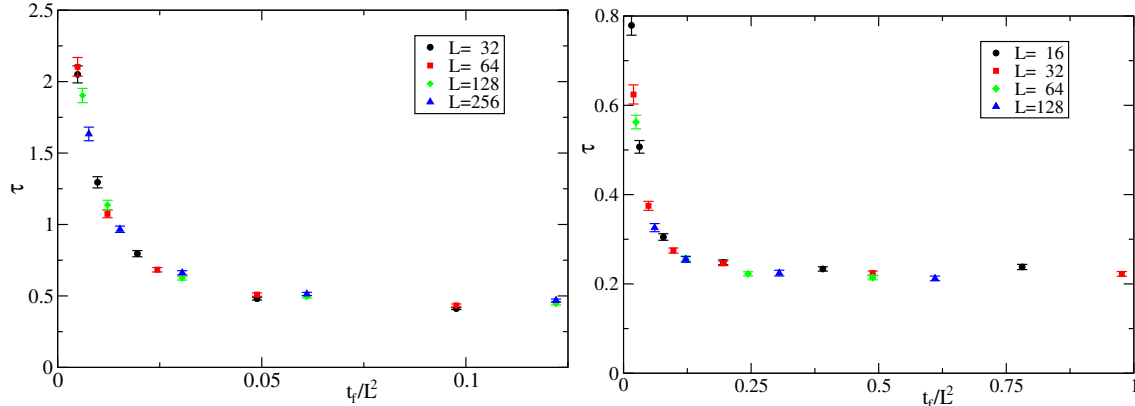


FIG. 1. Scaled integrated autocorrelation time for the observable  $O_3$ , left the two-dimensional Gaussian model, right the three-dimensional version.

From the plot we see a slight increase of  $\tau$  with increasing  $L$ . This will be studied below for a fixed value of  $t_f/L^2$  using higher statistics. The behavior of  $\tau_{int}$  for  $O_4$  is similar to that of  $O_3$ . In the case of  $O_1$  and  $O_2$  the behavior is different. For  $O_1$  we see an increase of  $\tau_{int}$  with increasing  $t_f$ . This increase is not dramatic and  $\tau_{int}$  seems to approach a plateau. For  $O_2$  we see a decrease of  $\tau_{int}$  with increasing  $t_f$ . It is however less pronounced as for  $O_3$  and  $O_4$ .

Next we performed simulations for  $t_f/L^2 = 125/4096 \approx 0.030517578\dots$  fixed. Measurements were performed after  $t_{meas} = 2t_f$ . Here we performed  $5 \times 10^6$  measurements for each lattice size. In addition to  $L = 32, 64, 128,$  and  $256$  we have simulated  $L = 512$ . The simulation for  $L = 512$  took 8 hours on one core of a Intel(R) Xeon(R) CPU E5-2660 v3 2.60GHz. The results for the integrated autocorrelation times are summarized in table I.

Looking at the numbers we see that for each observable, the integrated autocorrelation time is increasing with increasing lattice size. Roughly, doubling the lattice size, the autocorrelation times increase by an additive constant. I.e. it seems that the autocorrelation times increase logarithmically in the lattice size.

The CPU time that is used is proportional to the number of events. There is a small dependence on the mass and the lattice size for the number of events divided by  $t_f$ . Roughly this ratio equals 1.128 for all our masses and lattice sizes.

Note that our results are consistent with those of ref. [17], where the massless case was studied.

TABLE I. *Integrated autocorrelation times for  $t_f/L^2 = 125/4096 \approx 0.030517578\dots$ . The distance between two subsequent measurements is  $t_{\text{meas}} = 2t_f$ . For each  $L$ ,  $5 \times 10^6$  measurements are performed. The  $\tau$  are given in units of  $t_{\text{meas}}$ .*

$L$	$\tau_{\text{int},1}$	$\tau_{\text{int},2}$	$\tau_{\text{int},3}$	$\tau_{\text{int},4}$
32	7.23(5)	4.80(3)	3.70(3)	3.56(2)
64	8.03(5)	4.80(3)	3.90(4)	3.79(3)
128	8.74(5)	4.95(3)	4.10(4)	3.99(3)
256	9.47(6)	5.09(3)	4.26(4)	4.18(3)
512	10.13(6)	5.16(3)	4.42(4)	4.39(3)

TABLE II. *Autocorrelation times for the three-dimensional Gaussian model. Integrated autocorrelation times for  $t_f/L^2 = 1/4 = 0.25$ . The distance between two subsequent measurements is  $t_{\text{meas}} = L^3/32 = t_f L/8$ . For each  $L$ ,  $5 \times 10^6$  measurements are performed. The  $\tau$  are given in units of  $t_{\text{meas}}$ .*

$L$	$\tau_{\text{int},1}$	$\tau_{\text{int},2}$	$\tau_{\text{int},3}$	$\tau_{\text{int},4}$
16	17.32(15)	13.00(11)	7.85(9)	7.59(5)
32	16.71(14)	10.53(9)	7.56(8)	7.12(5)
64	17.08(14)	9.02(8)	7.45(8)	7.04(5)
128	16.82(14)	7.75(5)	7.29(7)	6.87(5)

## 2. Three dimensions

Next we simulated the three-dimensional Gaussian model. We simulated the linear lattice sizes  $L = 16, 32, 64$ , and  $128$  for various values of  $t_f$ . Similar to the two-dimensional case, we use the masses  $m = 0.6, 0.3, 0.15$ , and  $0.075$ . In Fig. 1 on the right, we give the integrated autocorrelation time of the observable  $O_3$ . Also in three dimensions it turns out that the curves for the different  $L$  fall approximately on top of each other for plotting  $\tau$  as a function of  $t_f/L^2$ . Since we have taken  $L \propto m^{-1}$ , it is likely, that actually  $m^2 t_f$  should be kept constant.

TABLE III. *Our results for the  $O(3)$ -invariant nonlinear  $\sigma$ -model on the square lattice.*

$\beta$	$E$	$\tau_E$	$\chi$	$\tau_\chi$	$N_{ev}/(L_0L_1)$
1.4	1.124340(23)	1.476(10)	78.65(10)	1.358(9)	0.954050(12)
1.5	1.203250(14)	1.507(11)	176.67(25)	1.597(13)	0.995291(9)
1.6	1.271421(7)	1.503(12)	447.42(69)	1.937(17)	1.033550(6)
1.7	1.3284761(35)	1.376(12)	1273.9(2.1)	2.306(26)	1.070078(4)
1.8	1.3758734(16)	1.256(11)	3841.2(7.0)	2.739(31)	1.105618(3)

As for two dimensions, we have measured the number of events per  $t$ . We get here  $\approx 1.38$ . For  $t_f/L^2 = 1/4 = 0.25$  we performed simulations with  $5 \times 10^6$  measurements. The results of these simulations are summarized in table II. In contrast to two dimensions, the autocorrelation times are slightly decreasing with increasing lattice size (decreasing mass).

### B. The $O(3)$ -invariant nonlinear $\sigma$ -model in two dimensions

We performed updates in the  $(0, 1)$ ,  $(0, 2)$  and  $(1, 2)$  planes of the spins in a fixed order. For each of the planes, we used  $t_f = L_0L_1$ . We simulated the model at  $\beta = 1.4, 1.5, 1.6, 1.7$ , and  $1.8$  on lattices of the linear size  $L = 68, 110, 190, 346$ , and  $646$ , respectively. Following ref. [13] the correlation length is  $\xi = 6.90(1), 11.09(2), 19.07(6), 34.57(7)$  and  $64.78(15)$  at these values of  $\beta$ , respectively. Consistent results are given in ref. [18].

Our results for the observables

$$E = \frac{1}{L^2} \sum_{x,\mu} \vec{s}_x \cdot \vec{s}_{x+\hat{\mu}}, \quad \chi = \frac{1}{L^2} \left( \sum_x \vec{s}_x \right)^2 \quad (25)$$

and the corresponding integrated autocorrelation times are summarized in table III. In the last column we give the average number of events divided by the number of sites for one cycle of three XY embeddings. The number slowly increases with increasing lattice size. This has to be taken into account when judging the performance of the algorithm. The fact that the number is close to one in all cases means that in one cycle, each site is touched roughly once.

In the case of the energy density  $E$ , the integrated autocorrelation time even decreases with increasing correlation length  $\xi$ . On the other hand, for the susceptibility  $\chi$ , the inte-

grated autocorrelation time is increasing with increasing  $\xi$ . Similar to the two-dimensional free field case, this increase seems to be logarithmic in  $\xi$ . Note that in ref. [3] slowing down with  $z \approx 1$  has been observed for the  $O(3)$ -invariant model on the three-dimensional simple cubic lattice. Furthermore one should notice that the single cluster algorithm [13] is more efficient than the event-chain Monte Carlo algorithm and on top of that provides variance reduced estimators for various observables.

### C. The $SU(3) \times SU(3)$ -invariant principal chiral model

Following Ref. [16, 19], we have investigated the performance of the event driven algorithm also in the  $SU(3) \times SU(3)$ -invariant principal chiral model. An update sequence is defined as a fixed random rotation matrix  $R$ , which is used in the event algorithm until a total rotation  $t_f$  has been performed. Then for the next update sequence a new  $R$  is used. In table IV we give the basic parameters of our runs. Again we confirm that the fluctuations of the results from various runs and trajectory lengths are compatible with the observed statistical noise and agree also with results from the literature [19].

We will focus on the following observables, constructed from fundamental and adjoint correlation functions [16]

$$G_F(x - y) = \langle \text{tr}(U_x^\dagger U_y) \rangle \quad ; \quad G_A(x - y) = \langle |\text{tr}(U_x^\dagger U_y)|^2 \rangle - 1. \quad (26)$$

using

$$E_F = \frac{1}{N} G_F(1, 0); \quad E_A = \frac{1}{N^2 - 1} G_A(1, 0) \quad (27)$$

$$\chi_F = \sum_{x \in \Lambda} G_F(x); \quad \chi_A = \sum_{x \in \Lambda} G_A(x) \quad (28)$$

as well as the correlation length

$$\xi_F = \frac{(\chi_F/F_F - 1)^{1/2}}{2 \sin(\pi/L)} ; \quad F_F = \sum_x e^{2\pi i x_0/L} G_F(x). \quad (29)$$

In this particular study, we also measure in time intervals which are smaller than  $t_f$  in order to reveal the scaling behavior with long update sequences. The results are shown in Fig. 2. We observe a rather weak dependence, with a shallow minimum, again for sequences with a length such that 0.1 to 1 events per site occur.

In Fig. 3 we plot the minimal integrated autocorrelation against the correlation length in Fig. 3. The scaling is compatible with  $z < 1$  for all observables that we have measured.

TABLE IV. Parameters of the runs for the principle chiral model.

$\beta$	$L$	$\xi_F$	$L/\xi_F$
1.5	32	3.01629(4)	10.6
1.65	64	5.4549(2)	11.8
1.825	128	11.679(6)	11.0
1.985	256	23.41(5)	10.9

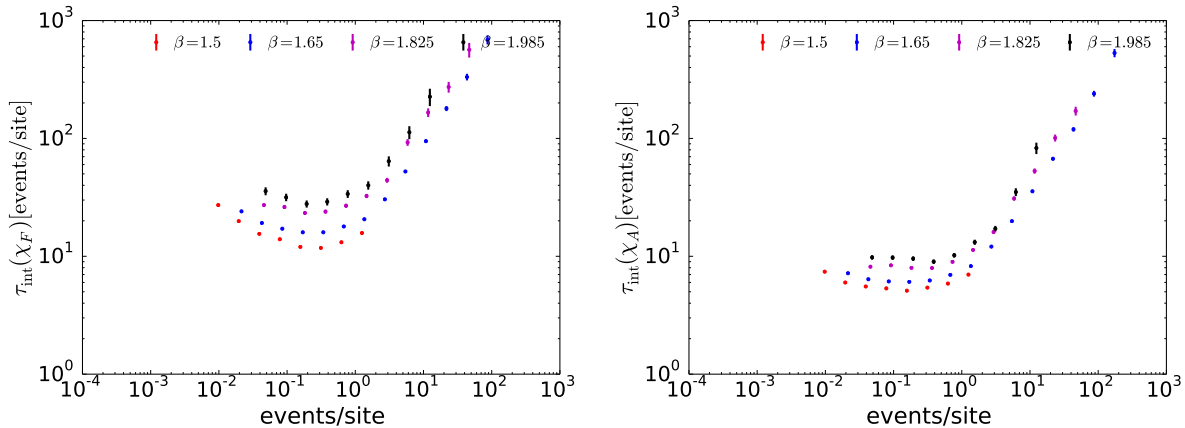


FIG. 2. Integrated autocorrelation time of the susceptibility as a function of the number of events within one update sequence divided by the lattice volume. On the left/right we give the results for the fundamental/adjoint representation. In both cases, we observe a weak dependence and a shallow minimum.

## V. CONCLUSIONS AND OUTLOOK

We applied the event-chain Monte Carlo algorithm [1–4] to asymptotically free models in two dimensions. In the literature, these models are considered as toy models of lattice QCD that allow for testing of algorithmic and theoretical ideas in a simplified setting. In a preliminary study, we applied the event-chain Monte Carlo to free field theory on a square and a simple cubic lattice. We find that critical slowing down is eliminated. This is quite astonishing for an algorithm, where local changes of the field variables are performed. Next we studied the two-dimensional XY-model. We do not discuss our results in detail. They corroborate the findings of [17]: At low temperatures, in the spin wave phase, slowing down

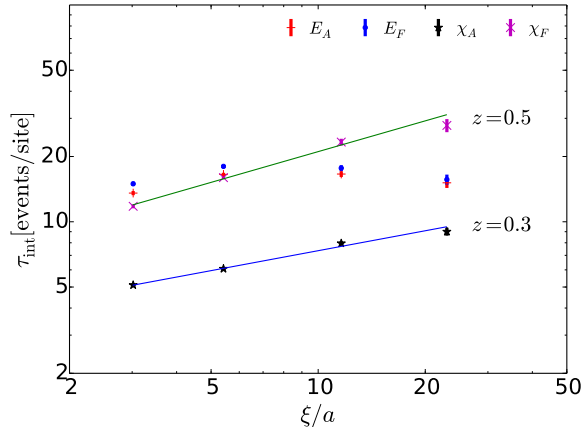


FIG. 3. Scaling of the integrated autocorrelation times with the correlation length. We observe dynamical critical exponents  $z$  well below 1 in all cases.

is eliminated, which is consistent with our free field theory result. On the other hand, in the high temperature phase, the physics is governed by vortices. Here we find slowing down with  $z \approx 2$ , even though the amplitudes of the integrated autocorrelation times are considerably reduced compared with the local Metropolis algorithm. One should note however that for this model the overrelaxation algorithm [14] gives  $z \approx 1$  in both phases and the cluster algorithm eliminates slowing down completely [13, 20]. In order to apply the event-chain Monte algorithm to the  $O(3)$ -invariant nonlinear  $\sigma$ -model and the  $SU(3) \times SU(3)$  chiral model, we use an embedding of the XY model. In the case of the  $O(3)$ -invariant model this simply means that one picks out two of the three components of the field. During one sequence of updates only these two components are updated. For the next sequence a new pair of components is taken. In the case of the  $SU(3) \times SU(3)$  principal chiral model the embedding is a bit more complicated. We follow ref. [9] who used such an embedding in the context of the multigrid algorithm. For details see section III C.

We find for both the  $O(3)$ -invariant nonlinear  $\sigma$ -model and the  $SU(3) \times SU(3)$  chiral model that critical slowing down is essentially eliminated. While this is certainly encouraging with regard to the application to lattice QCD, open questions remain. How should a coherent embedding of  $U(1)$  variables in the gauge theory look like? Will the event-chain Monte Carlo algorithm speed up the decorrelation of topological object that are present in QCD?

## Appendix A: Proof of stability

We have to show that the infinitesimal update by  $\epsilon$  preserves the target distribution

$$\pi(X) = \frac{1}{2VZ} \exp(-S[\phi]) \quad , \quad (\text{A1})$$

where  $Z$  is the partition function of the lattice model and the factors 2 and  $V$  give the number of possible values of  $\sigma$  and  $\tilde{x}$ . Let us write the update probabilities defined in section II as  $T(Y \leftarrow X)$ . Then stability means

$$\pi(Y) = \sum_X T(Y \leftarrow X) \pi(X) \quad , \quad (\text{A2})$$

where  $\sum_X$  is a short hand for the integral over the field  $\phi$  and the sums over  $\tilde{x}$  and  $\sigma$ . As a first step, we list the configurations  $X$  that can end up in a given  $Y = (\phi, \sigma, \tilde{x})$ , after an update step:

- $X_0$  given by  $\phi$  the same as for  $Y$ ,  $\sigma$  is replaced by  $-\sigma$  and the position of the walker  $\tilde{x}$  remains the same.
- $X_i$  given by  $\phi$  is the same as for  $Y$ ,  $\sigma$  is the same as for  $Y$  and  $\tilde{x} = y_i$ , meaning that the walker is hopping to its interaction partner  $y_i$ .
- $X_{n+1}$  given by  $\phi_{\tilde{x}} - \sigma\epsilon$ ,  $\phi_x$  with  $x \neq \tilde{x}$  are the same as for  $Y$ ,  $\sigma$  and  $\tilde{x}$  keep their value.

Hence eq. (A2) can be written as

$$\pi(Y) = \sum_{i=0}^{n+1} T(Y \leftarrow X_i) \pi(X_i) \quad . \quad (\text{A3})$$

Note that the probability density of  $X_i$  for  $i \leq n$  is the same as that of  $Y$ , since the field  $\phi$  is the same. The probability density of  $X_{n+1}$  is

$$\begin{aligned} \pi(X_{n+1}) &= \pi(Y) \exp \left[ - \sum_i [s_{i,x}(\phi_{\tilde{x}} - \sigma\epsilon) - s_{i,x}(\phi_{\tilde{x}})] \right] \\ &= \pi(Y) \left[ 1 + \sigma \sum_{i=0}^n \frac{\partial s_{i,\tilde{x}}}{\partial \phi_{\tilde{x}}} \epsilon + O(\epsilon^2) \right] \quad . \end{aligned} \quad (\text{A4})$$

Now let us work out the transition probabilities:

$$T(Y \leftarrow X_i) = 1 - p_i = \max \left[ 0, -\sigma \frac{\partial s_{i,\tilde{x}}}{\partial \phi_{\tilde{x}}} \epsilon \right] + O(\epsilon^2) \quad \text{for } i \leq n \quad . \quad (\text{A5})$$

Note that for  $i = 0$  the sign of  $\sigma$  changes, while for  $1 \leq i \leq n$  the hopping of the walker along with eq. (3) produces a minus sign. Finally

$$\begin{aligned} T(Y \leftarrow X_{n+1}) &= \prod_{i=0}^n p_i = \prod_{i=0}^n \min \left[ 1, 1 - \sigma \frac{\partial s_{i,\tilde{x}}}{\partial \phi_{\tilde{x}}} \epsilon \right] + O(\epsilon^2) \\ &= 1 + \sum_{i=0}^n \min \left[ 0, -\sigma \frac{\partial s_{i,\tilde{x}}}{\partial \phi_{\tilde{x}}} \epsilon \right] + O(\epsilon^2). \end{aligned} \quad (\text{A6})$$

Now we can put things together:

$$\begin{aligned} &\sum_{i=0}^n T(Y \leftarrow X_i) \pi(X_i) + T(Y \leftarrow X_{n+1}) \pi(X_{n+1}) \\ &= \pi(Y) \left( \sum_{i=0}^n \max \left[ 0, -\sigma \frac{\partial s_{i,\tilde{x}}}{\partial \phi_{\tilde{x}}} \epsilon \right] + O(\epsilon^2) \right) \\ &+ \pi(Y) \left( 1 + \sigma \sum_{i=0}^n \frac{\partial s_{i,\tilde{x}}}{\partial \phi_{\tilde{x}}} \epsilon + O(\epsilon^2) \right) \left( 1 + \sum_{i=0}^n \min \left[ 0, -\sigma \frac{\partial s_{i,\tilde{x}}}{\partial \phi_{\tilde{x}}} \epsilon \right] + O(\epsilon^2) \right) \\ &= \pi(Y) [1 + O(\epsilon^2)] \quad . \end{aligned} \quad (\text{A7})$$

Contributions  $O(\epsilon)$  exactly cancel each other.

- 
- [1] E. P. Bernard, W. Krauth, and D. B. Wilson, *Event-chain Monte Carlo algorithms for hard-sphere systems*, Phys. Rev. E **80**, 056704 (2009).
  - [2] M. Michel, J. Mayer, and W. Krauth, *Event-chain Monte Carlo for classical continuous spin models*, EPL (Europhysics Letters) **112**, 20003 (2015).
  - [3] Y. Nishikawa, M. Michel, W. Krauth, and K. Hukushima, *Event-chain algorithm for the Heisenberg model: Evidence for  $z \simeq 1$  dynamic scaling*, Phys. Rev. E **92**, 063306 (2015).
  - [4] S. Kapfer and W. Krauth, *Irreversible Local Markov Chains with Rapid Convergence towards Equilibrium*, Phys. Rev. Lett. **119**, 240603, (2017).
  - [5] R. H. Swendsen and J.-S. Wang, *Nonuniversal critical dynamics in Monte Carlo simulations*, Phys. Rev. Lett. **58**, 86 (1987).
  - [6] U. Wolff, *Collective Monte Carlo Updating for Spin Systems*, Phys. Rev. Lett. **62**, 361 (1989).
  - [7] J. Goodman and A. D. Sokal, *Multigrid Monte Carlo method. Conceptual foundations*, Phys. Rev. D **40**, 2035 (1989).
  - [8] R. C. Brower and P. Tamayo, *Embedded dynamics for  $\phi^4$  theory*, Phys. Rev. Lett. **62**, 1087 (1989).

- [9] T. Mendes, A. Pelissetto, and A. D. Sokal, *Multi-grid Monte Carlo via XY embedding. General theory and two-dimensional  $O(N)$ -symmetric non-linear  $\sigma$ -models*, Nucl. Phys. B **477**, 203 (1996).
- [10] M. Hasenbusch and K. Pinn, *Computing the roughening transition of Ising and solid-on-solid models by BCSOS model matching*, J. Phys. A **30**, 63 (1997).
- [11] M. Hasenbusch, *The Binder cumulant at the Kosterlitz-Thouless transition*, J. Stat. Mech.: Theor. Exp. (2008) P08003.
- [12] J. Balog, M. Niedermaier, F. Niedermayer, A. Patrascioiu, E. Seiler, and P. Weisz, *Comparison of the  $O(3)$  bootstrap  $\sigma$  model with the lattice regularization at low-energies*, Phys. Rev. D **60**, 094508 (1999).
- [13] U. Wolff, *Asymptotic freedom and mass generation in the  $O(3)$  nonlinear  $\sigma$ -model*, Nucl. Phys. B **334**, 581 (1990).
- [14] J. Apostolakis, C. F. Baillie, and G. C. Fox, *Investigation of the two-dimensional  $O(3)$  model using the overrelaxation algorithm*, Phys. Rev. D **43**, 2687 (1991).
- [15] U. Wolff, *Simulating the all-order strong coupling expansion III:  $O(N)$  sigma/loop models*, Nucl. Phys. B **824**, 254 (2010). [Erratum: Nucl. Phys. B **834**, 395 (2010)].
- [16] G. Mana, A. Pelissetto, and A. D. Sokal, *Multigrid Monte Carlo via XY embedding. II. Two-dimensional  $SU(3)$  principal chiral model*, Phys. Rev. D **55**, 3674 (1997).
- [17] Z. Lei and W. Krauth, *Irreversible Markov chains in spin models: Topological excitations*, EPL (Europhysics Letters) **121**, 10008 (2018).
- [18] J. Balog, M. Niedermaier, F. Niedermayer, A. Patrascioiu, E. Seiler, and P. Weisz, *Comparison of the  $O(3)$  bootstrap  $\sigma$  model with the lattice regularization at low-energies*, Phys. Rev. D **60**, 094508 (1999).
- [19] M. Hasenbusch and S. Meyer, *Multigrid acceleration for asymptotically free theories*, Phys. Rev. Lett. **68**, 435 (1992).
- [20] U. Wolff, *Collective Monte Carlo updating in a high precision study of the x-y Model*, Nucl. Phys. B **322**, 759 (1989).